*J. Am. Ceram. Soc.*, **93** [10] 3180–3189 (2010)
DOI: 10.1111/j.1551-2916.2010.03885.x

# Hydrolysis-Induced Aqueous Gelcasting of β-SiAlON–$SiO_2$ Ceramic Composites: The Effect of AlN Additive

Ibram Ganesh[†] and Govindan Sundararajan[*]

Centre for Advanced Ceramics, International Advanced Research Centre for Powder Metallurgy and New Materials (ARCI), Hyderabad 500 005, AP, India

**Dense β-SiAlON–$SiO_2$ ($SiO_2$ = 20, 40, 50, 60, and 80 wt%) ceramic composites have been prepared from β-$Si_4Al_2O_2N_6$ and fused silica by sintering at 1500°–1750°C for 3–4 h. For comparison purposes, a powder mixture consisting 60 wt% β-$Si_4Al_2O_2N_6$ and 40 wt% fused silica has been consolidated following a new near-net shape technique based on hydrolysis-induced aqueous gelcasting (GCHAS) and sintered for 3 h at 1750°C. In the GCHAS process, consolidation of suspensions containing 50 vol% solids was achieved by adding a polymerization initiator, a catalyst, and AlN powder equivalent to 1–5 wt% $Al_2O_3$. Thin-wall radomes consolidated by GCHAS (using AlN equivalent to 5 wt% $Al_2O_3$ in the suspension) have exhibited green strengths $>20$ MPa. The sintered materials were characterized for various properties including hardness, fracture toughness, mass loss, shrinkage, coefficient of thermal expansion, and dielectric constant. The $Si_2N_2O$ formed from a powder mixture of 60 wt% β-$Si_4Al_2O_2N_6$ and 40 wt% fused silica at 1750°C for 3 h exhibited a flexural strength of ~140 MPa, Young's modulus of 214 GPa, coefficient of thermal expansion of $3.5 \times 10^{-6}$ °$C^{-1}$, hardness of 1390 kg/$mm^2$, fracture toughness of 4.2 MPa · $m^{1/2}$, and a dielectric constant of 5.896 and tan δ of 0.002 at 17 GHz.**

## I. Introduction

Recently, β-SiAlON–$SiO_2$ ceramic composites have received a great deal of attention as materials of choice for certain high-speed (>Mach 5) radome applications.[1–3] Normally, high-speed radomes experience a transient temperature of about 1370°C together with high mechanical and aero-thermal loads in service. To withstand these severe environments while transmitting electromagnetic RADAR signals without any disturbance, the materials used for radome construction should have a low dielectric constant, a low loss tangent, a high flexural strength, high thermal shock resistance, high rain erosion, and particle impact resistance together with a high elastic modulus to keep the thin walls of the radome from buckling.[4,5] Although several materials such as fused silica,[6] Pyroceram 9606,[4] Rayceram 8,[4] barium aluminum silicate,[7] aluminum phosphate (commercially known as Cerablak™ and manufactured by Applied Thin Films Inc., Evanston, IL),[8,9] $SiO_2$–AlN ceramics,[10] $SiO_2$–BN ceramics,[11] reaction-bonded silicon nitride,[12] liquid-phase-sintered silicon nitride,[13] silicon nitride nanocomposite,[1] β-$Si_4Al_2O_2N_4$,[4,5] etc., have been investigated for these applications, only the β-SiAlON–$SiO_2$-based ceramic composites have received much importance as these latter composites possess the desired flexural strength and dielectric properties and can withstand high temperatures (>1300°C).[3] Recently, β-$Si_4Al_2O_2N_4$-based radomes have been successfully test fired for certain standard missile applications.[4,5] Despite their several useful properties, there is no straight forward fabrication route for dense components of β-SiAlON–$SiO_2$ ceramic composites.[2] This is due to the fact that β-$Si_4Al_2O_2N_4$ with >9 wt% $SiO_2$ cannot be prepared following a conventional reaction sintering of the precursor mixture consisting $Si_3N_4$, AlN, and $Al_2O_3$ powders, because they require an additional $SiO_2$ as one of the precursor materials.[4,5] As $SiO_2$ concentration increases in the precursor mixture, the diffusion paths between reactive $Si^{4+}$ and $Al^{3+}$ species also increase, which restricts the formation of the desired β-SiAlON phase during sintering. The presence of the required β-SiAlON phase in these composites is very important to have the desired flexural strength and fracture toughness properties.[14]

In a study, Gilde *et al.*,[1] have prepared a silicon oxy-nitride (SiON) nanocomposite with a dielectric constant of 4.78 at 25°C and 5.0 at 1000°C, and a loss tangent of 0.0014 at 25°C by calcining α-$Si_3N_4$ powder in an open-air atmosphere at 1700°C followed by fine grinding, recompaction, and resintering at >1800°C in $N_2$ atmosphere. However, this process does not yield the final product with consistent properties as its final chemical composition does not depend on the starting raw material composition; instead, it depends on the extent of oxidation that occurred upon calcination of α-$Si_3N_4$ powder in the air atmosphere. The oxidation of this powder is very sensitive to several processing parameters such as atmospheric humidity, the degree of agglomeration of powder particles, temperature fluctuations in furnace, etc. Despite these problems, in a recent study, Ganesh *et al.*,[2] have synthesized a ceramic composite with β-$Si_4Al_2O_2N_6$+9.0 wt% $SiO_2$ following a simple reaction sintering (for 4 h at 1750°C) of a precursor mixture, $Si_3N_4$/$Al_2O_3$ (= 1.5) using 7 wt% $Y_2O_3$ as a sintering aid (i.e., 1.5 $Si_3N_4$+$Al_2O_3$→β-$Si_4Al_2O_2N_6$+0.5 $SiO_2$). However, none of the combinations of $Si_3N_4$ and $Al_2O_3$ yield β-$Si_4Al_2O_2N_6$ with >9 wt% $SiO_2$. Of late, Advanced Materials Organization Inc., New York has started producing 25 cm height and 17.8 cm base diameter radomes with a chemical composition of 70% β-SiAlON+30% fused silica for vehicles that travel at a speed of >Mach 5. This ceramic composite exhibits a dielectric constant of 4.9 at 8.6 GHz, a flexural strength of 532 MPa, and a coefficient of thermal expansion (CTE) of $2.1 \times 10^{-6}$ °$C^{-1}$.[3] However, this process involves two very complicated, cumbersome, and expensive steps. In this process, initially, a green radome is produced by the gelcasting of a nonaqueous suspension containing precursor mixture plus 30% organic fugitive material, followed by drying and sintering of the green radome for 2–4 h at >1750°C under an $N_2$ pressure of 50–100 bar to form β-SiAlON with a porosity of 30%. Then, this porosity is filled with fused silica following a plasma spraying technique. Fused silica is added not only to reduce the dielectric constant from 7.3 to 4.2 but also to reduce the density of the radome from 3.2 to 2.2 g/$cm^3$, which is required for these high-speed radomes.[3] Nevertheless, introducing >30% porosity in the gelcast sintered β-SiAlON radomes by utilizing organic fugitive material is not an easy step particularly when the product yield is aimed at a high rate.

In view of the above, in this investigation, a systematic study was undertaken to prepare dense β-SiAlON–$SiO_2$ ceramic

---

W.-C. Wei—contributing editor

Manuscript No. 27094. Received November 12, 2009; approved April 19, 2010.

[*] Member, The American Ceramic Society.

[†] Author to whom correspondence should be addressed. e-mail: ibram_ganesh@yahoo.com

composites with a wide chemical composition following a conventional powder-processing route. Initially, a β-$Si_4Al_2O_2N_6$ powder was prepared by the extrusion of the precursor mixture paste followed by drying, reaction sintering, and fine grinding.[15–20] The fine-ground β-$Si_4Al_2O_2N_6$ powder was mixed with different amounts of fused silica (0, 20, 40, 50, 60, 80, and 100 wt%) and then die-pressed and sintered for 3–4 h at 1500°–1750°C.[17] For comparison purposes, a powder mixture consisting 60 wt% β-$Si_2Al_2O_2N_6$, and 40 wt% fused silica was also consolidated following an hydrolysis-induced aqueous gelcasting (GCHAS) process.[18,20–23] In the GCHAS process, suspensions with 50 vol% solids were utilized. To accomplish consolidation, a polymerization initiator, a catalyst, and AlN powder equivalent to 1–5 wt% $Al_2O_3$ on the powder weight basis have been introduced into the particulate suspensions. The fully dried green consolidates were then sintered for 3 h at 1750°C in an $N_2$ atmosphere to achieve the desired densification. All the sintered materials were thoroughly characterized in order to understand the effects of added fused silica and AlN into particulate suspension on the physical, thermal, mechanical, and dielectric properties of β-$Si_4Al_2O_2N_6$ and of sintered ceramic composites consolidated by the GCHAS route.

## II. Experimental Section

### (1) Synthesis of β-$Si_4Al_2O_2N_6$ Powder

The starting raw materials used in this study were α-$Si_3N_4$ (SicoNide-P95H, VESTA Ceramics AB, Sweden, BET surface area—6.51 $m^2$/g and average particle/agglomerate size, APS—17.77 μm), α-$Al_2O_3$ (HP Grade, ACC India Limited, Thane, India, BET SA—1.24 $m^2$/g and APS—1.39 μm), AlN (Grade AT, H.C. Stark, Goslar, Germany, BET SA—6.72 $m^2$/g and APS—7.62 μm), $Y_2O_3$ (Rhodia Inc., Phoenix, AZ, BET SA—3.41 $m^2$/g and APS—3.23 μm), and fused silica (Chettinad Quartz Products Private Ltd., Chennai, India, APS—19.95 μm). Before use, the as-purchased AlN powder was treated in an ethanol solution of ortho-phosphoric acid and aluminum dihydrogen phosphate at 80°C for 24 h in order to passivate it against hydrolysis.[16] It is known that AlN decomposes into ammonia and aluminum hydroxide when it comes into contact with water ($AlN + 3H_2O \rightarrow Al(OH)_3 + NH_3$).[24,25] If AlN is utilized as one of the starting precursor materials without passivating it against hydrolysis in the processing of SiAlON following an aqueous colloidal processing route, this AlN will be decomposed in the suspension. This decomposition causes coagulation of the suspension in the vessel used for powder deagglomeration purpose, setting of the suspension within the vessel, and the overall change in the targeted chemical composition.[26,27]

In a typical experiment, a powder mixture of 64.33% α-$Si_3N_4$, 23.36% α-$Al_2O_3$, 9.37% AlN (surface passivated against hydrolysis),[16] and 7% $Y_2O_3$ was kneaded in a conventional dough-making machine (Sigma Kneader, Prigmayers India Private Limited, Mumbai, India) with 3 wt% methyl cellulose, 2 wt% polyethylene glycol (PEG 400) (both are GR grade procured from Loba Chemie, Mumbai, India), and about 30 wt% double-distilled water to obtain an easily extrudable dough.[15] The resultant dough was then extruded through an indigenously designed and fabricated stainless steel die using a ram-type extruder at a rate of 50 mm/min under a pressure of 10–20 kg/$cm^2$ to form extrudates of about 5 mm thickness.[15] These extrudates were allowed to dry in an open-air atmosphere over night under ambient conditions, which were then cut into 5–6 mm length pieces. These cut pieces were then subjected to binder removal for 2 h at 500°C and then sintered for 4 h at 1675°C under an $N_2$ atmosphere of about 800 torr to form β-$Si_4Al_2O_2N_6$ extrudates (Fig. 1(a)).[17–19] During sintering, these extrudates were covered with a powder mixture of 50% $Si_3N_4$+50% BN to protect them against decomposition.[17] The sintered extrudates were crushed in an hammer mill followed by wet grinding in a stainless steel jar (350 mm diameter and 400 mm height) using stainless steel balls of about 12 mm as well as 25 mm diameters by maintaining the 1:8 weight ratio of charge to balls. This milling operation was continued till the average particle size of β-$Si_4Al_2O_2N_6$ reached about 3 μm.

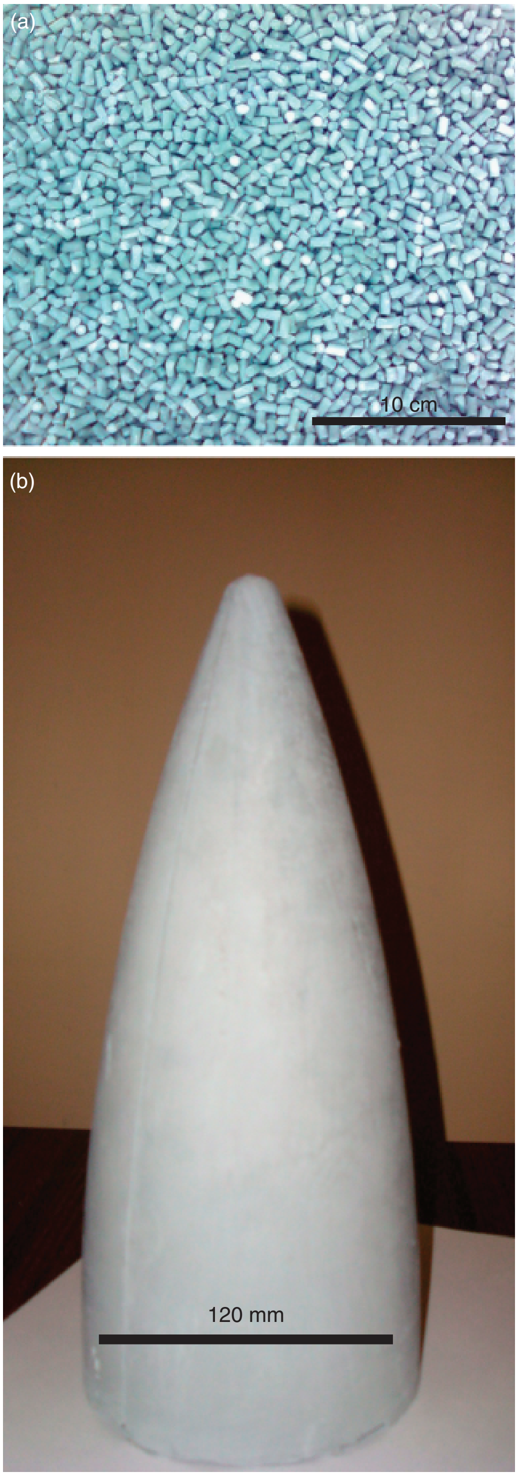

**Fig. 1.** (a) Extrudates of β-$Si_4Al_2O_2N_6$ formed by the reaction sintering of a precursor mixture consisting α-$Si_3N_4$, α-$Al_2O_3$, surface passivated AlN against hydrolysis, and $Y_2O_3$ (7 wt%) at 1675°C for 4 h. (b) A digital photograph of the green radome shape consolidated by hydrolysis-induced aqueous gelcasting of a suspension containing 50 vol% solids loading and AlN equivalent to 5 wt% $Al_2O_3$ on the total powder basis.

### (2) Synthesis of β-$Si_4Al_2O_2N_6$–$SiO_2$ Ceramic Composites

A conventional dry-powder pressing technique was used to make these ceramic composites. Before pressing into pellets of

30 or 90 mm diameter × ~10 mm height under a pressure of 200 MPa, ~200 g of powder mixture containing the requisite amounts of β-$Si_4Al_2O_2N_6$ and fused silica, ~60 g of 5 wt% aqueous PVA solution and ~200 g of $ZrO_2$ cylindrical pebbles (10 mm diameter and 12 mm length) were suspended in ~200 mL of toluene in a 500 mL alumina bowl and were ground for 30 min in a planetary ball mill (Retsch GmbH, Haan, Germany). The resultant dough was separated from the toluene solution, dried at ~85°C for 12 h in an electrically heated hot-air oven. This dried mass was passed through a −30 to +100 BSS mesh to form granules before pressing into pellets. Binder burnout was operated on all die-pressed samples for 2 h at 500°C before sintering for 3–4 h at 1500°–1750°C in nitrogen atmosphere (>900 torr) by covering them in a powder bed of 50 wt% $Si_3N_4$+50 wt% BN.[17–19]

### *(3) Colloidal Processing of β-SiAlON–$SiO_2$ Ceramic Composites*

In a typical experiment, a powder mixture consisting 60 wt% β-$Si_4Al_2O_2N_6$+40 wt% fused silica was dispersed in an aqueous solution of 8.6 wt% methacrylamide, 2.8 wt% methylenebisacrylamide, and 8.6% *n*-vinylpyrrolidinone, with the help of Dolapix CE64, an amino alcohol-based cationic dispersant (Zchimmer & Schwarz, Berlin, Germany) used at a ratio of 10 μL/g of powder mixture to achieve a suspension with 50 vol% solids loading.[27] This aqueous solution has been termed as NVPNCPM (*n*-vinylpyrrolidone nonconvectional premix) solution.[17–23] In order to optimize the amount of Dolapix CE 64 (dispersant) required to obtain suitable particulate suspensions, initially a separate study was conducted aiming at low viscous (<450 MPa · s) suspensions with solids loading as high as 50 vol%. In this study, Dolapix CE 64 was used at a ratio of 5–35 μL/g of powder mixture. Only the suspension containing the ratio of 10 μL/g of powder mixture could accommodate the solids loading up to 50 vol% and exhibited a viscosity of <450 MPa · s. It has been reported that suspensions with a viscosity of <450 MPa · s and solids loading of >48 vol% are required to fabricate defect-free thin-wall/complex-shaped ceramic components following advanced net-shaping colloidal routes such as either aqueous gelcasting or hydrolysis-induced aqueous gelcasting.[17–23] The minimum solids loading in the suspensions required to fabricate radome shapes without any difficulty was found to be 48 vol% in the present study. When this solids loading was <48 vol%, the suspensions took more time to get gelled and the gelled parts were always found to be cracked as the mold mandrel could not allow the part to shrink to get enough handling strength. In contrast, when the solids loadings were >50 vol%, the viscosity of the suspensions was increased to >500 MPa · s. It was found to be quite difficult to remove the entrapped air/gas bubbles fully from a suspension having >500 MPa · s viscosity.[17–23,27] The suspensions containing 50 vol% powders composition and alumina balls (with a charge to balls weight ratio of 1:3) in polypropylene bottles were rolled on a roller mill for about 18 h to accomplish the powder deagglomeration process. To the resultant suspensions, the as purchased pure AlN (equivalent to 1–5 wt% of $Al_2O_3$ on total powder weight basis) powder without any surface modification was introduced and the deagglomeration process was continued for a further 2 h.[18,20–23] Thus, the obtained suspensions were added with a polymerization initiator (10 wt% aqueous solution of ammonium persulfate, APS) and a catalyst (as purchased tetramethylethylenediammine, TEMED) at a ratio of 4 and 2 μL/g of particulate suspension, respectively, and then degassed for ~2 min by vacuum pumping. Both APS and TEMED are of GR grade procured from Loba Chemie. These degassed suspensions were then cast into an indigenously designed and fabricated split-type Teflon-lined aluminum radome-shape mold, and inserted aluminum solid mandrel into the suspension. After mandrel insertion, the suspension was allowed to completely gel under ambient conditions in the mold.[18–27] Always, some excess suspension was poured in the mold so as to overflow this excess suspension from top of the mold along with air/gas bubbles (if any leftover after vacuum pumping) while inserting the mandrel into the suspension in the mold. Always, some rectangular (60 mm × 30 mm × 30 mm) bars were also cast along the radome shapes to check the condition of gel before removing the mandrel from the radome mold.[18] After confirming the gelation of suspension, the mandrel was removed from the mold and then was filled with polyethylene glycol-400 (PEG400) (AR grade, Loba Chemie).[26] Owing to high chemical potential, water moves from gel (i.e., from wet radome) into the PEG. After about 2 h, the PEG was removed from mold, and then the wet-green radome was removed from the mold by simply tilting the mold up-side down. This radome was then placed in a humidity-controlled oven (Model: LHL-113; Espec Corporation, Osaka, Japan) that was preset at 40°C and 90% RH.[22] After drying for 24 h at 40°C, the temperature in the humidity oven was raised to 70°C and then to 90°C. At each of these temperatures, the radome was held for ~24 h. One of the thus-dried green radome shapes is shown in Fig. 1(b). All the GCHAS green samples were then subjected to binder removal for 2 h at 500°C and then sintered for 3 h at 1750°C under about 900 torr $N_2$ pressure.

### *(4) Material Characterization*

A Gemini Micromeritics BET surface area analyzer (Model 2360, Micromeritics, Norcross, GA) was used for specific surface area measurements of the powders. Surface area was measured by nitrogen physisorption at liquid nitrogen temperature (−196°C) by taking 0.162 $nm^2$ as the area of cross section of $N_2$ molecule.[28] Particle size analysis of the powders was performed using a light scattering equipment (Coulter LS 230, London, U.K., Fraunhofer optical model). The viscosity of suspensions was measured using a rotational Rheometer (Bohlin C-VOR Instruments, Worcestershire, U.K.).[20,21] The measuring configuration adopted was a cone and plate (4°, 40 mm, and gap of 150 μm), and the flow measurements were conducted between 0.1 and 800 $s^{-1}$. Before carrying out the viscosity measurements, bubbles were removed by slow speed agitation from the suspensions.

The XRD patterns were recorded using a Bruker (Karlsruhe, Germany) D8 advanced system with a diffracted beam monochromated Cu$K\alpha$ (0.15418 nm) radiation source.[29] Crystalline phases were identified by comparison with PDF-4 reference data from the International Centre for Diffraction Data (ICDD).[29] Bulk density, apparent porosity, and water absorption capacity of sintered samples were measured according to the Archimedes principle (ASTM C372) using a Mettler balance and the attachment (AG 245, Mettler Toledo, Greifensee, Switzerland). On an average, three density measurements were performed on each sample in this study (±0.01 SD).[18] The microstructure of sintered ceramic composites was examined using a scanning electron microscope (S-3400N, SEM, Hitachi, Tokyo, Japan). The flexural strength of 60 × 4 × 3 mm size samples was measured using the four-point bend test (JIS-R1601).[20,21] These samples were cut from sintered rectangular bars of ~90 mm length and ~30 mm width and ~10 mm thickness. Six to eight samples were examined per case and all the readings were averaged out (±3 SD). The fracture toughness value ($K_{Ic}$) was calculated on the basis of the indentation method [$K_{Ic} = Ha^{1/2} \times 0.203\ (C/a)^{-3/2}$].[30] Here, $2a$ represents Vickers indent diagonal length, $2C$ the resulted crack length, and $H$ is a Vickers hardness ($H_V = \text{kg/mm}^2 = 10$ MPa). Five to six samples were examined per case; in order to check the reproducibility of fracture toughness, results and all the readings were averaged out (±0.2 SD). The required hardness, crack, and diagonal length data were collected using a microhardness tester (Leitz Wetzler, Siegmund-Hiepe-Strasse, Germany) by holding the indenter tip (having 137°) under the load of 2 kg for 20 s on the surface of the sample polished to a mirror finish. More than 20 indentations were performed to estimate a hardness value. Dielectric properties were measured using a Hewlett Packard HP 8510 Network Analyzer (Santa Rosa, CA) using 15.8 mm × 7.8 mm × 1.7 mm size specimen fixed in mild steel flanges (32.5 mm × 32.5 mm × 1.7 mm) according to the Nicolson and Ross technique.[17–19,31]

## III. Results and Discussion

Table I lists the powder compositions used to prepare various ceramic composites following the conventional dry-powder pressing route, the values of green density of dry-powder pressed pellets, and of bulk density, apparent porosity, and linear shrinkage of ceramic composites sintered for 4 h at 1500°–1675°C and for 3 h at 1750°C. Different codes are given to the powder compositions for easy identification purposes. SS in the sample codes indicates the ceramic composites made from a powder mixture of β-$Si_4Al_2O_2N_6$ and fused silica, and the numbers 0–100 represent the fused silica content in the starting powder compositions. The following conclusions can be drawn from the data of Table I. (1) There is a gradual increase in the value of green density with the increase of β-$Si_4Al_2O_2N_6$ content in the composite. This is due to the fact that fused silica possesses a lower density (2.2 g/cm$^3$) than that of β-$Si_4Al_2O_2N_6$ (3.10 g/cm$^3$). (2) In general, the compositions with fused silica $\geq$50 wt% (i.e., SS-50, SS-60, and SS-80) underwent early densification even at a temperature of 1500°C when compared with β-$Si_4Al_2O_2N_6$-rich compositions (SS-20 and SS-40) and with the fused silica (SS-100). The latter compositions underwent desired densifications only when sintered at 1750° and 1675°C, respectively. The early densification of fused silica-rich compositions when compared with pure fused silica could be attributed to the eutectic melts formed among $Y_2O_3$, $Al_2O_3$, and $SiO_2$ at 1350°C during sintering.[14] (3) The β-$Si_4Al_2O_2N_6$ densified from its powder (i.e., SS-0) exhibited considerably low apparent porosity values ($<$0.5%) after sintering at 1675° and 1750°C. The remaining composites exhibited significantly higher apparent porosity values (up to 41.2%) even after sintering at the desired temperature. (4) Among all the sintered samples, pure fused silica (SS-100) underwent the highest shrinkage (12.41%) after sintering for 4 h at 1675°C. The remaining sintered composites exhibited linear shrinkage values comparable with those values reported for similar materials prepared by dry-powder pressing followed by sintering.[17,18]

XRD patterns of sintered SS-0 to SS-100 are presented in Fig. 2. It can be seen that SS-0 shows XRD lines primarily due to β-$Si_4Al_2O_2N_6$ (ICDD File No.: 00-048-1616) together with some minor peaks that are attributed to $Y_2SiAlO_5N$ (ICDD File No.: 00-048-1627) and other un-known phases.[17,18] The phase $Y_2SiAlO_5N$ forms due to the reactions that occur among $Y_2O_3$, α-$Al_2O_3$, and surface $SiO_2$ of α-$Si_3N_4$ during sintering.[14] Although, SS-20 also exhibited XRD lines primarily due to the β-$Si_4Al_2O_2N_6$ phase with a slight shift in their 2θ values, it has also exhibited some minor peaks due to a new phase, $Si_2N_2O$ (ICDD File No.: 00-047-1627). On the other hand, SS-40 exhibited XRD lines exclusively due to this new phase $Si_2N_2O$. The sintered fused silica revealed XRD lines exclusively due to the cristobalite phase indicating that it stabilizes into the cristobalite phase during sintering. Although SS-50 was prepared from a powder mixture consisting 50 wt% β-$Si_4Al_2O_2N_6$ and 50 wt% fused silica, it exhibited XRD lines primarily due to fused silica-derived cristobalite together with some minor lines due to starting β-$Si_4Al_2O_2N_6$ and due to newly formed phase, $Si_2N_2O$. On the other hand, both SS-60 and SS-80 exhibit strong XRD lines due to cristobalite phase together with some minor lines due to β-$Si_4Al_2O_2N_6$ and $Si_2N_2O$ phases. In these composites, interestingly, the starting material β-$Si_4Al_2O_2N_6$ exhibited stronger peaks than the new phase, $Si_2N_2O$. The considerable amount of viscous liquid melt formed in these two composites during sintering normally does not allow moving relatively largely isolated β-$Si_4Al_2O_2N_6$ particles with enough speed to react with and form the $Si_2N_2O$ phase.[2,3]

As mentioned in the introduction section, certain high-speed ($>$Mach 5) radomes see a transient temperature of about 1300°C in service. Therefore, the construction materials of these

Table I. Properties of Sintered (1500°–1750°C for 3–4 h) Ceramic Composites Consolidated by the Conventional Dry-Powder Pressing Route

| Ceramic composite‡ | Sintering temperature (°C/h) | SS-0 | SS-20 | SS-40 | SS-50 | SS-60 | SS-80 | SS-100 |
|---|---|---|---|---|---|---|---|---|
| Starting raw materials composition (wt%) | — | 100-β-$Si_4Al_2O_2N_6$ | 80-β-$Si_4Al_2O_2N_6$+ 20-fused silica | 60-β-$Si_4Al_2O_2N_6$+ 40-fused silica | 50-β-$Si_4Al_2O_2N_6$+ 50-fused silica | 40-β-$Si_4Al_2O_2N_6$+ 60-fused silica | 20-β-$Si_4Al_2O_2N_6$ +80-fused silica | 100-Fused silica |
| Green density (g/cm$^3$) | — | 1.72 | 1.89 | 1.83 | 1.66 | 1.52 | 1.63 | 1.14 |
| Bulk density (g/cm$^3$) | 1500/4 | — | — | 2.00 | 2.45 | 2.48 | 2.26 | — |
| Apparent porosity (%) | | — | — | 29.26 | 2.15 | 3.29 | 4.72 | — |
| Linear shrinkage (%) | | — | — | Slightly swelled | 3.23 | 4.83 | 5.06 | — |
| Bulk density (g/cm$^3$) | 1600/4 | 2.84 | 2.31 | 1.69 | 1.69 | 1.49 | 1.10 | 1.86 |
| Apparent porosity (%) | | 6.86 | 26.88 | 41.22 | 31.79 | 32.86 | 3.97 | 16.43 |
| Linear shrinkage (%) | | 3.26 | 2.89 | Slightly swelled | Swelled | 0.5 (Swelled) | Swelled | 8.34 |
| Bulk density (g/cm$^3$) | 1675/4 | 3.09 | 2.56 | 1.72 | Melted | Melted | Melted | 1.97 |
| Apparent porosity (%) | | 0.45 | 17.53 | 41.01 | Melted | Melted | Melted | 10.72 |
| Linear shrinkage (%) | | 5.03 | 4.40 | 1.23 | Melted | Melted | Melted | 12.41 |
| Bulk density (g/cm$^3$) | 1750/3 | 3.21 | 2.84 | 2.51 | Melted | Melted | Melted | 1.54 |
| Apparent porosity (%) | | 0.01 | 2.47 | 5.44 | Melted | Melted | Melted | 19.80 |
| Linear shrinkage (%) | | 5.60 | 5.33 | 10.68 | Melted | Melted | Melted | Melted |

†Values were obtained as mentioned in "Section I." ‡In the sample codes, SS indicates a ceramic composite formed from a mixture of β-$Si_4Al_2O_2N_6$ and fused silica, and the numbers 0–100 represent the fused silica content in starting material composition.

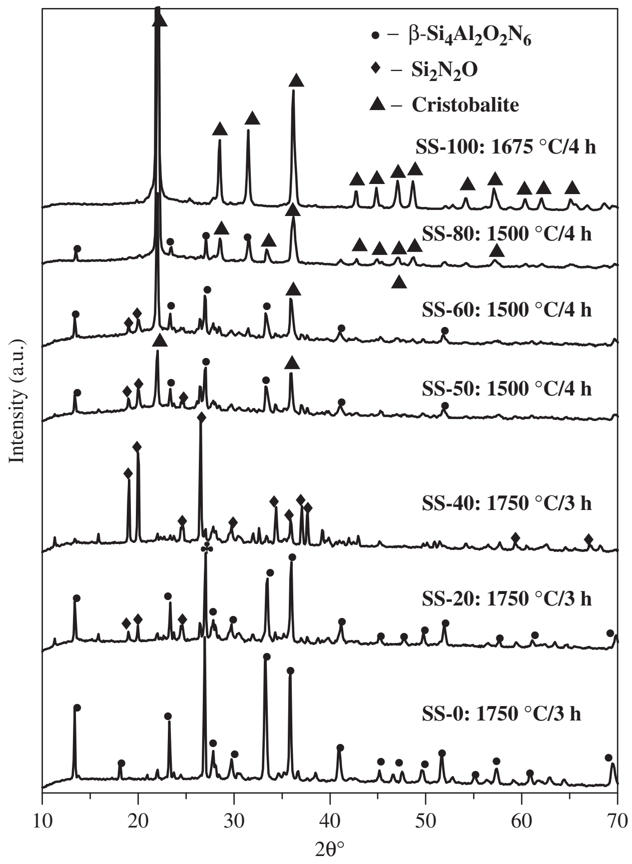

**Fig. 2.** XRD patterns of SS-0, SS-20 to SS-80 ceramic composites, and SS-100 sintered at different conditions (Table I).

radomes should be able to withstand a temperature of at least 1300°C and also should have dielectric constants preferably $<6$.[1–15] Among the various ceramic composites prepared in this study (listed in Table I), only SS-40 is expected to meet both these requirements, i.e., the high-temperature-withstanding capability and the dielectric constant as it needed the highest sintering temperature (1750°C) used in this study for achieving the maximum densification and it contains the maximum amount of fused silica, a low dielectric constant material among composites sintered at 1750°C. Considering these facts, SS-40 was selected to consolidate following the advanced new net-shaping technique, GCHAS as this technique allows the fabrication of thin-wall radomes with near-net shapes and with very high green strengths (i.e., >20 MPa).[18,20–23]

Table II lists the precursor mixture compositions used in the GCHAS process, the values of viscosity of suspensions (at a shear rare, $\gamma$, of 141 $s^{-1}$), the setting time of suspensions, as well as the values of green density, percentage linear shrinkage occurred upon casting and drying, and green flexural (four-point bend) strength of consolidates. In the given sample codes, SS40 indicates the ceramic composites made from a powder mixture of 60 wt% β-$Si_4Al_2O_2N_6$ and 40 wt% fused silica, and the numbers 1–5 represent the AlN added to suspensions equivalent to the weight percent of $Al_2O_3$. The viscosity of the suspensions considerably decreased with increasing concentrations of AlN in the suspension, reaching the lowest value of 406 MPa·s for SS40-5. Usually, when AlN is introduced into aqueous suspensions, the following three reactions occur:

$$AlN + 2H_2O \rightarrow AlO(OH) + NH_3 \quad (1)$$

$$NH_3 + H_2O \rightarrow NH_4OH \quad (2)$$

$$AlO(OH) + H_2O \rightarrow Al(OH)_3 \quad (3)$$

It consumes water, releases ammonia, and forms aluminum hydroxides. This released ammonia changes the pH and rheological characteristics of aqueous suspensions.[24,25] In the present case, the generated ammonia gas increases the pH of the suspension away from the iso-electric-point of the dispersed powders, thereby increasing the stability and fluidity of suspensions by decreasing their viscosities.[18,25] Further, the pH of the suspension was found to be slightly increased from about 8.5 to 10 with the increase of AlN concentration in the suspension equivalent to 1–5 wt% of $Al_2O_3$. The suspension, SS40-1, took about 11 min to completely convert into a gel after introducing a polymerization initiator, a catalyst, and the AlN equivalent to 1 wt% of $Al_2O_3$. On the other hand, the suspension, SS40-5, took only about 5 min after introducing the polymerization initiator, the catalyst, and the AlN equivalent to 5 wt% of $Al_2O_3$. The suspension introduced with APS and TEMED at a ratio of 4 and 2 μL/g of particulate suspension, respectively, and with AlN equivalent to 5 wt% $Al_2O_3$ was found to be best for fabricating thin-wall radome shapes (Fig. 1(b)) without any difficulty. These results indicate that AlN concentration in the suspension drastically reduces the setting time of suspensions under ambient conditions.[18,25] In all the three events (Eqs. (1)–(3)), water is consumed and solids content is increased. These events support the early setting of suspensions when higher amounts of AlN are introduced into them.[24] The flexural strength of green bodies also increased with the AlN content. In GCHAS process, strength not only comes from polymerization of organic monomers present in the suspension but also by the cementing action of boehmite formed by the hydrolysis of AlN added to the suspension.[18,20–23] The generated boehmite connects the ceramic particles into a stiff body and the content of this boehmite increases with the concentration of AlN in the suspension.[24] Because of the involvement of both the strengthening mechanisms, SS40-5 exhibited the highest green strength value of 20.25±2.66 MPa. Green ceramics with a flexural strength of even 18 MPa have been successfully green machined to obtain the desired shape following usual machining operations.[27] Green machining can in turn greatly reduces the expen-

**Table II. Properties of Suspensions and of Green Consolidates Obtained by the GCHAS Route**

| | Precursor mixture | | | | | | | | |
|---|---|---|---|---|---|---|---|---|---|
| Ceramic composite[‡] | β-$Si_4Al_2O_2N_6$ (%) | Fused silica (%) | A-AlN (%) | α-$Al_2O_3$ (wt%) to be formed upon hydrolysis and firing of added A-AlN | Suspension viscosity at $\gamma = 141\ s^{-1}$ (MPa·s) | Suspension setting time (min) | Green strength (MPa) | Green density ($g/cm^3$) | Linear shrinkage from casting to drying (%) |
| SS40-1 | 59.51 | 39.67 | 0.80 | 1 | 503 | ~11 | 14.13±1.87 | 1.83±0.06 | 2.32±0.23 |
| SS40-2 | 59.03 | 39.35 | 1.61 | 2 | 467 | ~10 | 15.32±2.17 | 1.82±0.04 | 2.33±0.11 |
| SS40-3 | 58.52 | 39.01 | 2.47 | 3 | 433 | ~8 | 16.72±2.32 | 1.82±0.05 | 2.33±0.32 |
| SS40-4 | 58.06 | 38.70 | 3.24 | 4 | 416 | ~6 | 18.42±2.48 | 1.81±0.03 | 2.34±0.27 |
| SS40-5 | 57.56 | 38.37 | 4.06 | 5 | 409 | ~5 | 20.25±2.66 | 1.80±0.05 | 2.34±0.21 |

[†] Values were obtained as explained in "Section I". Suspensions were prepared by dispersing powder mixtures of 60 wt% β-$Si_4Al_2O_2N_6$+40 wt% fused silica in NVPNCPM (*n*-vinylpyrrolidone nonconvectional premix solution) using 10 μL Dolapix CE 64 dispersing agent/g of powder mixture. [‡] In sample codes, SS-40 indicates the ceramic composite formed from a powder mixture of 60 wt% β-$Si_4Al_2O_2N_6$+40 wt% fused silica; the numbers 1–5 represent the AlN content equivalent to 1–5 wt% $Al_2O_3$ on total powder basis added to the suspensions; A-AlN stands for as purchased AlN powder, which was not passivated against hydrolysis. GCHAS, hydrolysis-induced aqueous gelcasting.

sive post sintering machining operation, and thereby the manufacturing cost.[18,26]

A gradual decrease in the values of green density (from 1.83 to 1.80 g/cm$^3$) and a gradual increase in the values of percentage linear shrinkage (from 2.32% to 2.34%) with the increasing AlN concentration in suspension can be observed from the data presented in Table II. The decrease of green density with the increasing AlN concentration in the suspension could be attributed to the amount of $NH_3$ gas released in the suspension due to AlN hydrolysis (Eq. (1)).[24] Normally, some of the ammonia gas remains entrapped in the suspension having a viscosity of >400 MPa · s, even after vacuum pumping. This entrapped gas leads to the formation of fine pores in the green bodies, which in turn is responsible for lower densities of consolidates.[24] Nevertheless, these green density values are well-comparable with the one (1.82 g/cm$^3$) measured for a dry-powder-pressed sample having the same composition of β-$Si_4Al_2O_2N_6$ and fused silica (SS-40).

XRD patterns of SS40-1 to SS40-5 sintered for 3 h at 1750°C are presented in Fig. 3. XRD lines only due to $Si_2N_2O$ (ICDD File No.: 00-047-1627) are seen in all the spectra indicating that the available 40 wt% fused silica in the reaction mixture could not be converted into the cristobalite phase; instead, it reacted with β-$Si_4Al_2O_2N_6$ and led to the formation of a new phase, $Si_2N_2O$. The boehmite and/or $Al(OH)_3$ formed by the hydrolysis of AlN in the suspension appear to have little effect on the phase evolution in these ceramic composites. In fact, this boehmite and/or $Al(OH)_3$ are supposed to react with fused silica and/or the surface $SiO_2$ of β-$Si_4Al_2O_2N_6$ during sintering and a led to the formation of certain alumino-silicate phases such as, mullite.[32] However, no XRD lines due to any of the alumino-silicate phases are noted in these XRD spectra. The reason for the absence of these phases could be that the phases formed and/or their crystallite sizes are below the detection limit of the XRD instrument.[28]

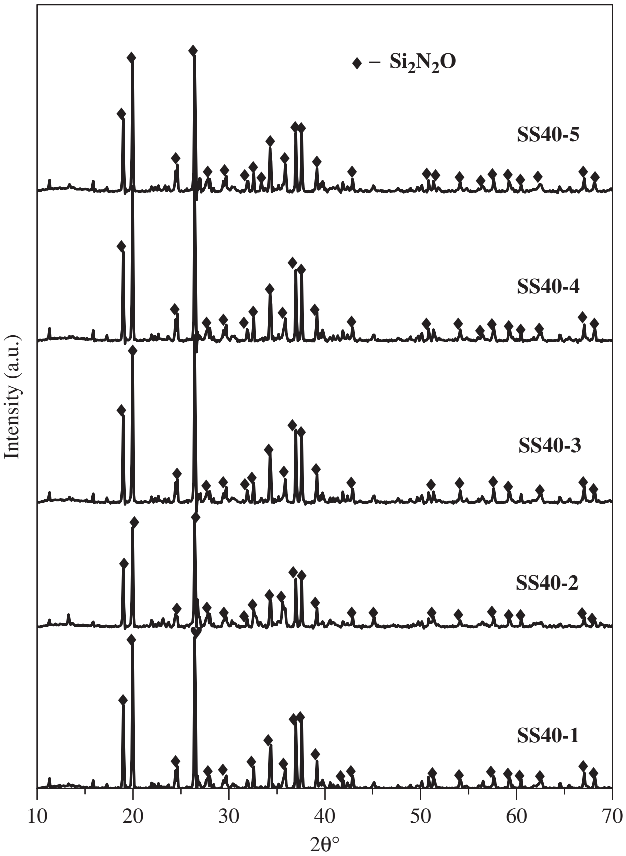

**Fig. 3.** XRD patterns of SS40-1 to SS40-5 ceramic composites sintered for 3 h at 1750°C (Table II).

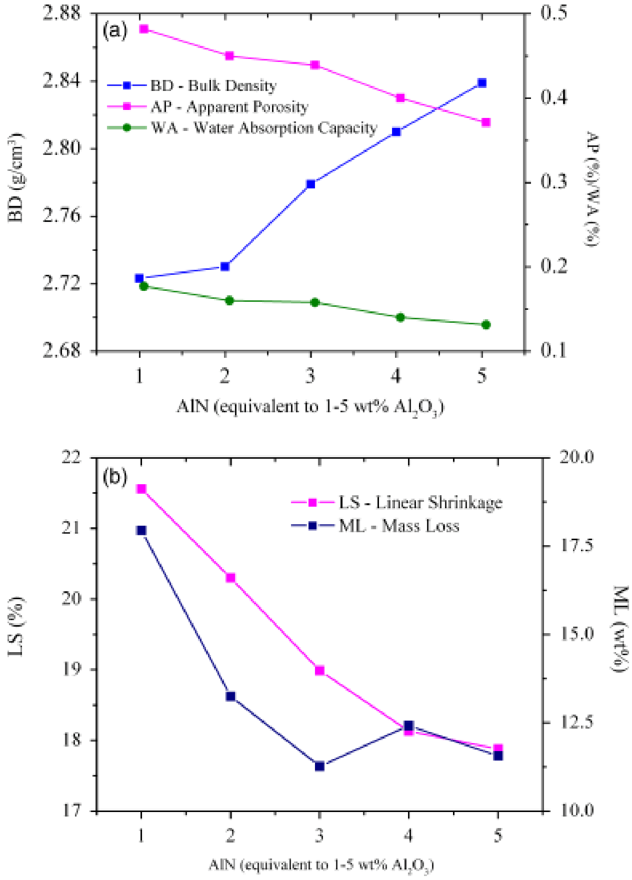

**Fig. 4.** (a) Bulk density, apparent porosity, and water absorption capacity, and (b) linear shrinkage and mass loss of SS40-1 to SS40-5 sintered for 3 h at 1750°C.

The SS-40 consolidated by the dry-powder pressing route followed by sintering for 3 h at 1750°C exhibited a bulk density of 2.51 g/cm$^3$, apparent porosity of 5.445%, water absorption capacity of 2.168%, linear shrinkage of 10.68%, hardness of 1319 kg/mm$^2$, fracture toughness of 3.22 MPa · m$^{1/2}$, and flexural strength of 113 MPa. On the other hand, the pure stoichiometric β-$Si_4Al_2O_2N_6$ formed by the reaction sintering (at 1675°C for 4 h) of extrudates consisting α-$Si_3N_4$, α-$Al_2O_3$, surface passivated AlN against hydrolysis, and $Y_2O_3$ (7 wt %) exhibited a bulk density of 3.08 g/cm$^3$, apparent porosity of 0.19%, water absorption capacity of 0.12%, linear shrinkage of 14%, hardness of 1317 kg/mm$^2$, fracture toughness of 3.30 MPa · m$^{1/2}$, and flexural strength of 216 MPa. Although the hardness and fracture toughness values of these two different sintered materials are comparable, there is a large gap between their flexural (four-point bend) strength values (β-$Si_4Al_2O_2N_6$ had a strength of 226 MPa, whereas the SS-40 (i.e., $Si_2N_2O$) had only 113 MPa). The kinds of bonds and the amounts of porosity present in these sintered materials could be responsible for the difference in the flexural strength values measured.[14]

The values of bulk density, apparent porosity, and water absorption capacity, and the values of linear shrinkage and mass loss of SS40-1 to SS40-5 sintered for 3 h at 1750°C are plotted in Figs. 4(a) and (b), respectively. Their corresponding hardness and fracture toughness values, and the flexural strength and Young's modulus values are plotted in Figs. 5(a) and (b), respectively, as a function of the amount of AlN added to their corresponding suspensions. In general, all these properties appear to be very sensitive to the AlN concentration in the suspensions. There is a significant difference between the apparent porosity and water absorption capacity values measured for SS-40, and SS40-1 to SS40-5, although all these samples were sintered under identical conditions. Furthermore, there is a

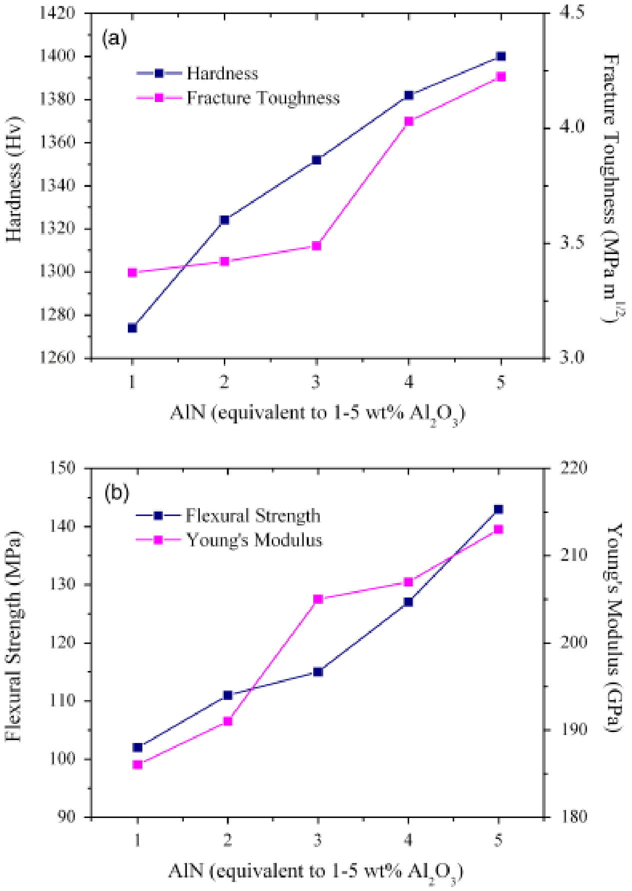

**Fig. 5.** (a) Hardness and fracture toughness, and (b) flexural strength and Young's modulus of SS40-1 to SS40-5 sintered for 3 h at 1750°C.

gradual increase in the values of bulk density, hardness, fracture toughness, flexural strength, and Young's modulus, and a concurrent decrease in the values of apparent porosity, water absorption capacity, linear shrinkage, and mass loss with the increasing concentration of AlN in the suspension. Hardness is increased from 1270 to 1390 kg/mm$^2$, fracture toughness from 3.35 to 4.2 MPa · m$^{1/2}$, flexural strength from 90 to 140 MPa, and Young's modulus from 184 to 213 GPa, and on the other hand, the linear shrinkage is decreased from 22.5% to 18% and mass loss from 18% to 11%. The increased amounts of new alumino-silicate chemical bonds formed by the reactions occurred between aluminum hydroxides derived from AlN added to the suspensions, and the $Si_2N_2O$ (Fig. 2) could be responsible for the above observed changes in the sintered properties. Nevertheless, further work is under active progress to fully establish the underlying mechanisms in improving the above properties due to AlN addition into the suspensions.

The fractured SEM micrographs of sintered SS-40 and SS40-1 to SS40-5 are presented in Figs. 6(a)–(f), respectively. Purposefully, micrographs were recorded at pores in order to understand the features of grains that were not broken upon fracture. A considerable amount of porosity together with elongated grains and fused mass is observed in all these micrographs. The observed porosity justifies the mass loss that occurred upon sintering. Relatively more elongated grains are seen in SS40-1 to SS40-5 in comparison with SS-40. The EDAX study revealed that the elongated grains are made of $Si_2N_2O$, and the fused mass is made of cristobalite and/or fused silica. Furthermore, as none of the SS40-1 to SS40-5 sintered ceramics revealed the apparent porosity values >1%, the porosity appearing in these micrographs could be a closed one, where water could not be entered while estimating apparent porosity values following the water displacement method. In line to its bulk density and apparent porosity properties, the micrograph of SS-40 reveals the presence of relatively large size pores when compared with those present in SS40-1 to SS40-5. Furthermore, an increased connectivity among the elongated grains can be seen with the increasing amount of AlN in suspension. These improved connections could be responsible for superior properties measured for SS40-5 in comparison with those measured for SS-40, and SS40-1 to SS40-4.

Dielectric constant profiles of SS40-1 to SS40-5 ceramic composites sintered for 3 h at 1750°C are presented in Fig. 7 in the frequency range of 16.8–17.2 GHz. A quite stable and low dielectric constant values (in the range of 5.896–6.313) can be seen at 17 GHz frequency. The dielectric constant value of 6.03 was measured at 17 GHz frequency for sintered SS-40, whereas the values 7.3 and 3.9 were reported for the stoichiometric β-$Si_4Al_2O_2N_6$ formed by the reaction sintering of $Si_3N_4$, $Al_2O_3$, AlN, and $Y_2O_3$ precursor mixture and for sintered fused silica, respectively.[17,33,34] The dielectric constant of any ceramic material is not only influenced by its chemical composition but also by the several other properties such as, frequency of the applied field, temperature of the dielectric, humidity, crystal structure, and other external factors including porosity.[35,36] Furthermore, as the applied frequency is varied through 16.8 to 17.2 GHz at an ambient temperature in this study, the measured dielectric constant values could be mainly contributed by

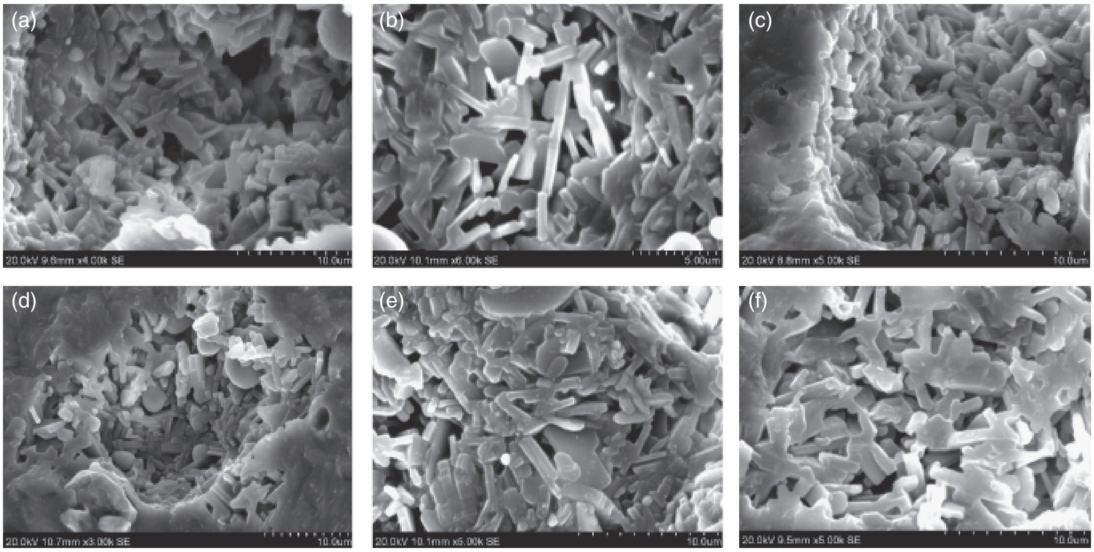

**Fig. 6.** The sintered SEM micrographs of SS-40 (a), SS40-1 (b), SS40-2 (c), SS40-3 (d), SS40-4, (e), and SS40-5 (f).

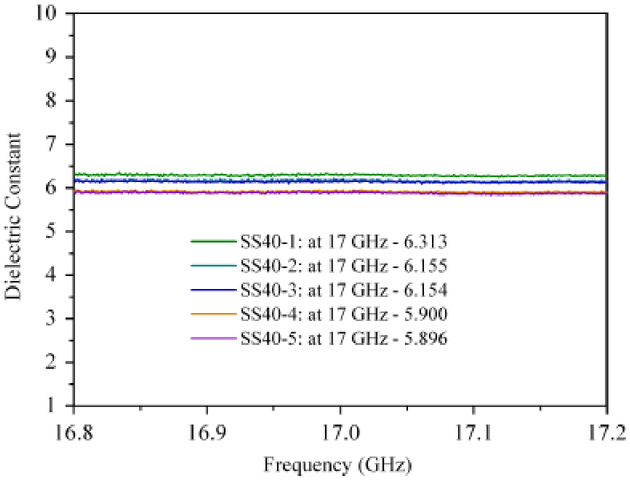

**Fig. 7.** Dielectric constant profiles of SS40-1 to SS40-5 sintered for 3 h at 1750°C.

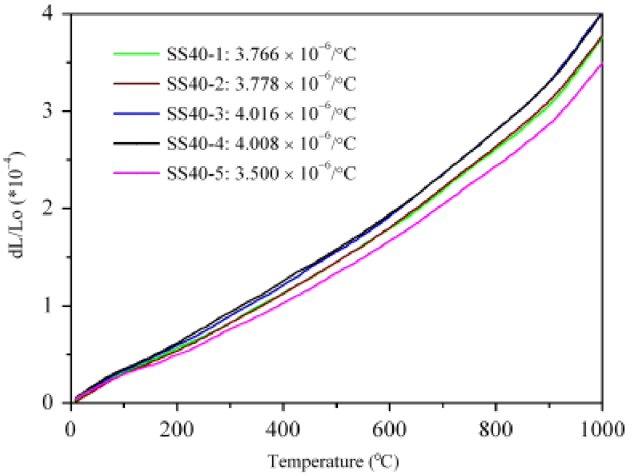

**Fig. 8.** Coefficient of thermal expansion profiles SS40-1 to SS40-5 sintered for 3 h at 1750°C.

electronic and ionic polarization mechanisms only.[36] In addition to these, a gradual decrease in the dielectric constant value with the increasing amount of AlN can also be seen. Although, porosity decreases the dielectric constant of a sintered material, in the present case, the dielectric constant values were decreased with the decreasing porosity, which indicates that the changes noted in the dielectric constant values with the increasing concentration of AlN are mainly due to the changes that occurred in the chemical composition but not due to the changes that occurred due to their physical properties such as porosity. The decreasing trend (Fig. 4(b)) in degree of mass loss occurred in SS40-1 to SS40-5 sinters with the increasing amount of AlN in the suspension. The decreasing of degree of mass loss means an increasing of the degree of $SiO_2$ in SS40-1 to SS40-5 sinters as mass loss in SiAlON-based ceramics occurs mainly due to the evaporation of $SiO_2$ at elevated temperatures.[27] As the dielectric constant of $SiO_2$ is lower than that of β-$Si_4Al_2O_2N_6$ and $Si_2N_2O$, the increased amount of $SiO_2$ with AlN amount has caused the reduction in the dielectric constant of SS40-1 to SS40-5 ceramics. In addition to this, the dielectric constant (5.5) of aluminosilicate compounds such as mullite to be formed due to reactions occurring between the alumina derived from AlN in the suspension and fused silica and/or β-$Si_4Al_2O_2N_6$ is lower than that of β-$Si_4Al_2O_2N_6$ (7.4).[9,33,34] From these dielectric constant results, it can be concluded that by mixing 40 wt% fused silica to the β-$Si_4Al_2O_2N_6$ powder, the dielectric constant of their sintered composite product could be reduced from 7.313 (measured for β-$Si_4Al_2O_2N_6$) to 6.313 (measured for SS-40), which can be further reduced to 5.896 (measured for SS40-5) by the addition of AlN equivalent to 5 wt% $Al_2O_3$ in its starting suspension. Dielectric constant values in the range of 6.84–7.46 were reported for gelcast β-$Si_4Al_2O_4N_6$ ceramics.[2–7,17–19] A dielectric constant value of 4.78 at 25°C and 5.0 at 1000°C, and a loss tangent value of 0.0014 at 25°C were reported for SiON nanocomposite.[1] A dielectric constant value of 6.3 was reported for β-$Si_4Al_2O_2N_6$-9 wt% $SiO_2$ composite formed at 1750°C.[2] A dielectric constant value of 4.9 at 8.6 GHz was reported for a ceramic composite having a chemical composition of 70%

**Table III. Sintered Properties of SS40-5 and of Various Commercial Radome Materials**

| Materials trade and manufacturer's name | Basic chemical composition | Bulk density (g/cm$^3$) | Elastic modulus (GPa) | Flexural strength (MPa) | Coefficient of thermal expansion, CTE ($10^{-6}$ °C$^{-1}$) | Dielectric permittivity (ε′) | Tan δ | References |
|---|---|---|---|---|---|---|---|---|
| Pyoceram 9606 (Corning Inc., Corning, NY, USA) | Cordierite | 2.6 | 121 | 240 | 4.7 | 5.5 | 0.0005 | Kirby *et al.*[4] |
| Fused silica (Ceradyne Inc., Costa Mesa, CA) | $SiO_2$ | 2 | 37 | 43 | 0.7 | 3.3 | 0.003 | Nei *et al.*[6] |
| IRBAS (Lockheed Martin Inc.) | $Si_3N_4$ | 3.18 | 280 | 550 | 3.2 | 7.6 | 0.002 | Mangels and Mikijelj[37] |
| Ceralloy 147-31N (Ceradyne Inc.) | $Si_3N_4$ | 3.21 | 310 | 800 | — | 8 | 0.002 | Mangels and Mikijelj[37] |
| Ceralloy 147-01EXP (Ceradyne Inc.) | Reaction bonded $Si_3N_4$ | 1.8–2.5 | 50–200 | 180 | 3.1 | 4–6 | 0.002–0.005 | Mangels and Mikijelj[37] |
| β-SiAlON (ORNL) | β-$Si_4Al_2O_2N_6$ | 3.02 | 230 | 260 | 4.1 | 7.4 | 0.003 | Kirby and colleagues[4,6] |
| Cerablak™, Applied Thin Films Inc., Lockheed Martin Corporation, Bethesda, MD | $Al_2O_3$–$P_2O_5$ composite | 2.0–2.5 | — | — | 5.0 | 3.3–5 | — | Mora and colleagues[8,9] |
| Invisicone (AMO) | β-SiAlON–$SiO_2$ | 2.2 | — | 532 | 2.0 | 4.9 | 0.002 | Paquette[3] |
| SS40-5 (material of this study, Table II) | $Si_2N_2O$ | 2.81 | 214 | 140 | 3.50 | 5.896 | 0.002–0.003 | — |

ORNL, Oak Ridge National Laboratory, Oak Ridge, TN, USA; AMO, Advanced Materials Organization; CTE, coefficient of thermal expansion.

SiAlON+30% $SiO_2$.[3] Thus, the dielectric constant values (5.896–6.313) measured in this study for SS40-1 to SS40-5 prepared by simple GCHAS are well comparable with those values reported in the literature for similar kind of materials that were prepared following quite complicated procedures involving quite capital-intensive equipments.[3]

The CTE profiles recorded between 30° and 1000°C for SS40-1 to SS40-5 sintered for 3 h at 1750°C are presented in Fig. 8. These ceramics revealed CTE values in the range of $3.50-4.016 \times 10^{-6}$ °C$^{-1}$. There is a gradual increase of CTE from 3.766 to $4.016 \times 10^{-6}$ °C$^{-1}$ with the increase of AlN concentration in the suspension from 1 to 3 equivalent wt% of $Al_2O_3$, and then there is a decreasing trend in the value reaching the lowest value of $3.50 \times 10^{-6}$ °C$^{-1}$ when the concentration of AlN increased the equivalent to 5 wt% $Al_2O_3$. The variations in the CTE values measured for these ceramics can be mainly attributed to the changes that occurred to their chemical composition by the incorporation of AlN into their starting suspensions. The CTE value of $4.1 \times 10^{-6}$ °C$^{-1}$ for a gelcast β-$Si_4Al_2O_2N_6$ and of $2.1 \times 10^{-6}$ °C$^{-1}$ for a ceramic composite of β-SiAlON+30% $SiO_2$ between 25° and 1000°C are reported.[3–5] The CTE values in the range of $3.532-4.657 \times 10^{-6}$ °C$^{-1}$ between 30° and 700°C have been reported for β-$Si_{6-z}Al_zO_zN_{8-z}$ in which z varied from 1.5 to 4.[17] Thus, the CTE values measured for SS40-1 to SS40-5 are quite comparable with the values reported for similar kind of materials in the literature.[4,5,17,26]

Table III presents the basic chemical composition, bulk density, elastic modulus, flexural strength, CTE, dielectric permittivity, and tan δ of SS40-5 and of several other commercial radome materials. Material trade names as well as the supplier's and their corresponding country names are also presented in this table. In general, all the radome materials exhibited reasonably low bulk density values (<3.2 g/cm$^3$), which are recommended for high-speed radome materials. It can be seen that among various materials, only the $Si_3N_4$-and β-SiAlON-based materials exhibited relatively higher elastic modules and flexural strength values.[37] Except Ceralak™ ($5.0 \times 10^{-6}$ °C$^{-1}$), Pyroceram 9606 ($4.7 \times 10^{-6}$ °C$^{-1}$), and β-SiAlON ($4.1 \times 10^{-6}$ °C$^{-1}$), all other materials exhibited relatively low CTE values ($<3.5 \times 10^{-6}$ °C$^{-1}$). As far as the important dielectric permittivity property is concerned, the fused silica appears to be the best as it has the value of 3.3. The highest permittivity values are reported for β-SiAlON (7.4), and the $Si_3N_4$-based materials, IRBAS (7.6) and Ceralloy 147-31N (8).[37] Nevertheless, all these materials exhibited considerably low tan δ values (i.e., <0.003). When compared with other materials, the SS40-5 possesses elastic modulus and flexural strength values that are almost three times higher than those of fused silica. The dielectric permittivity value of SS40-5 was measured to be 5.896, which is less than that of β-$Si_4Al_2O_2N_6$ (7.4), IRBAS (7.6), and Ceralloy 147-31N (8). Based on these permittivity and strength properties together with the high temperature (>1300°C) withstanding and radome shape-forming capability, this SS40-5 can be considered for certain high-speed radome applications.[1–15]

## IV. Conclusions

The following conclusions can be drawn from the above study: dense stoichiometric β-$Si_4Al_2O_2N_6$ extrudates with >90% β-SiAlON phase can be prepared by reaction sintering of α-$Si_3N_4$, α-$Al_2O_3$, surface passivated AlN against hydrolysis, and $Y_2O_3$ (7 wt%) precursor mixture for 4 h at 1675°C. The dry-powder-pressed composites of fine β-$Si_4Al_2O_2N_6$ and fused silica powders can be sintered for 3–4 h at 1500°–1750°C to form dense ceramic composites with $SiO_2$ in the range of 20–80 wt%. Defect-free green radome shapes with green strengths >20 MPa can be consolidated following a net-shape technique based on GCHAS process by involving an AlN equivalent 5 wt% $Al_2O_3$ in the starting particulate suspension together with a polymerization initiator and a catalyst. The $Si_2N_2O$ formed at 1750°C for 3 h from a powder mixture of 60 wt% β-$Si_4Al_2O_2N_6$ and 40 wt% fused silica exhibits flexural strength values more than three times of sintered bulk fused silica, and a dielectric constant value less than that of stoichiometric β-$Si_4Al_2O_2N_6$.

## Acknowledgment

Authors express their gratitude to their colleagues at ARCI for their contributions to this study.

## References

[1] G. Gilde, P. Patel, C. Hubbard, B. Pothier, T. Hynes, W. Croft, and J. Wells, "SiON Low Dielectric Constant Ceramic Nanocomposite"; U.S. Patent No.: 5,677,252, October 14, 1997.

[2] I. Ganesh, N. Thiyagarajan, D. C. Jana, P. Barik, and G. Sundararajan, "An Aqueous Gelcasting Route to Dense β-$Si_4Al_2O_2N_6$–0.5$SiO_2$ Ceramics," *J. Am. Ceram. Soc.*, **91** [5] 1566–71 (2008).

[3] D. G. Paquette, "Method of Making a Radar Transparent Window Material Operable Above 2000°C"; U.S. Patent No.: 5,627,542, May 6, 1997, and references therein.

[4] K. W. Kirby, A. T. Jankiewicz, M. A. Janney, C. Walls, and D. Kupp, "Gelcasting of GD-1 Ceramic Radomes"; pp. 287–95 *Proceedings of the 8th DoD Electromagnetic Windows Symposium*, St. Louis, MO, 2000.

[5] M. A. Janney, C. A. Walls, D. M. Kupp, and K. W. Kirby, "Gelcasting SiAlON Radomes," *Am. Ceram. Soc. Bull.*, **83**, 9201–6 (2004).

[6] J. T. Neil, L. J. Bowen, and B. E. Michaud, "Fused Silica Radome"; U.S. Patent No.: 4,949,095, August 14, 1990.

[7] D. W. Freitag and K. K. Richardson, "BAS Reinforced *In-Situ* with Silicon Nitride"; U.S. Patent No.: 5,358,912, October 25, 1994.

[8] F. G. Mora, K. C. Goretta, D. Singh, J. L. Routbort, S. Sambasivan, K. A. Steiner, J. Adabie, and K. K. Rangan, "High-Temperature Deformation of Amorphous $AlPO_4$-Based Nano-Composites," *J. Eur. Ceram. Soc.*, **26**, 1179–83 (2006).

[9] Y. Wang and J. Liu, "Aluminum Phosphate-Mullite Composites for High-Temperature Radome Applications," *Int. J. Appl. Ceram. Technol.*, **6** [2] 190–4 (2009).

[10] J. Wu, J. Guo, and B. Li, "Preparation and Properties of $SiO_2$ Matrix Composites Doped with AlN Particles," *J. Mater. Sci.*, **35** [19] 4895–900 (2000).

[11] G. Wen, G. L. Wu, T. Q. Lei, Y. Zhou, and Z. X. Guo, "Co-Enhanced $SiO_2$–BN Ceramics for High-Temperature Dielectric Applications," *J. Eur. Ceram. Soc.*, **20** [12] 1923–8 (2000).

[12] M. Y. Hsieh, "Silicon Nitride Having Low Dielectric Loss"; U.S. Patent No.: 4,642,299, February 10, 1987.

[13] M. Y. Hsieh, H. Mizuhara, and P. W. Smith, "Pressureless Sintered Silicon Nitride as a Promising Candidate for Radome Materials"; *17th Symposium on Electromagnetic Windows*, Atlanta, GA., July 25–27, 1984.

[14] S. Hampshire, H. K. Park, D. P. Thompson, and H. K. Jack, "α-SiAlON," *Nature (London)*, **274**, 880–2 (1978).

[15] B. P. Saha, Roy Johnson, I. Ganesh, G. V. N. Rao, S. Bhattacharjee, and Y. R. Mahajan, "Thermal Anisotropy in Sintered Cordierite Monoliths," *Mater. Chem. Phys.*, **67** [1–3] 140–5 (2001).

[16] I. Ganesh, S. M. Olhero, A. A. Branca, M. R. Correia, G. Sundararajan, and J. M. F. Ferreira, "Chemisorption of Phosphoric Acid and Surface Characterization of as Passivated AlN Powder Against Hydrolysis," *Langmuir*, **24** [10] 5359–65 (2008).

[17] I. Ganesh, N. Thiyagarajan, D. C. Jana, Y. R. Mahajan, and G. Sundararajan, "Influence of Chemical Composition and $Y_2O_3$ on Sinterability, Dielectric Constant and CTE of β-SiAlON," *J. Am. Ceram. Soc.*, **91** [1] 115–20 (2008).

[18] I. Ganesh, "Near-Net Shape β-$Si_4Al_2O_2N_6$ Parts by Hydrolysis Induced Aqueous Gelcasting Process," *Int. J. Appl. Ceram. Technol.*, **6** [1] 89–101 (2009).

[19] I. Ganesh, N. Thiyagarajan, D. C. Jana, Y. R. Mahajan, and G. Sundararajan, "An Aqueous Gelcasting Process for β-$Si_4Al_2O_2N_6$ Ceramics," *J. Am. Ceram. Soc.*, **91** [9] 3121–4 (2008).

[20] I. Ganesh, S. M. Olhero, P. M. C. Torres, F. J. Alves, and J. M. F. Ferreira, "Hydrolysis Induced Aqueous Gelcasting for Near-Net Shaping of ZTA Ceramic Composites," *J. Eur. Ceram. Soc.*, **29**, 1393–401 (2009).

[21] I. Ganesh, G. J. Reddy, G. Sundararajan, S. M. Olhero, P. M. C. Torres, and J. M. F. Ferreira, "Hydrolysis Induced Aqueous Gelcasting of $MgAl_2O_4$ Spinel," *Int. J. Appl. Ceram. Technol.*, doi:10.1111/j.1744-7402.2010.02520.x (2010).

[22] I. Ganesh, G. Sundararajan, S. M. Olhero, P. M. C. Torres, and J. M. F. Ferreira, "A Novel Colloidal Processing Route to Alumina Ceramics," *Ceram. Int.*, **36**, 1357–64.

[23] I. Ganesh, G. J. Reddy, S. M. Olhero, P. M. C. Torres, and J. M. F. Ferreira, "Influence of Processing Route on Micro-Structure and Mechanical Properties of $MgAl_2O_4$ Spinel," *Ceram. Int.*, **36**, 473–82 (2010).

[24] T. Kosmac, S. Novak, and M. Sajko, "Hydrolysis-Assisted Solidification (HAS): A New Setting Concept for Ceramic Net-Shaping," *J. Eur. Ceram. Soc.*, **17**, 427–32 (1997).

[25] I. Ganesh, N. Thiyagarajan, D. C. Jana, P. Barik, J. M. F. Ferreira, and G. Sundararajan, "Dense β-SiAlONs Consolidated by a Modified Hydrolysis Assisted Solidification Route," *J. Eur. Ceram. Soc.*, **28** [4] 879–85 (2008).

[26] M. A. Janney, C. A. Walls, D. M. Kupp, and K. W. Kirby, "Gelcasting SiAlON Radomes," *Am. Ceram. Soc. Bull.*, **7**, 9201–6 (2004).

[27] M. A. Janney, S. D. Nunn, C. A. Walls, O. O. Omatete, R. B. Ogle, G. H. Kirby, and A. D. McMillan, "Gelcasting"; pp. 1–15 in *The Handbook of Ceramic Engineering*, Edited by M. N. Rahman. Marcel Dekker, New York, 1998.

[28] S. Brunauer, P. H. Emmett, and E. Teller, "Adsorption of Gases in Multimolecular Layers," *J. Am. Chem. Soc.*, **60**, 309–19 (1938).

[29] H. P. Klug and L. E. Alexander, "X-Ray Diffraction Procedure for Polycrystalline and Amorphous Materials," *J. Appl. Crystallogr.*, **8**, 573–4 (1975).

[30] G. R. Anstis, P. Chantikul, B. R. Lawn, and D. B. Marshall, "A Critical Evaluation of Indentation Techniques for Measuring Fracture Toughness. I. Direct Crack Measurements," *J. Am. Ceram. Soc.*, **64**, 533–8 (1981).

[31] A. M. Nicolson and G. F. Ross, "Measurement of the Intrinsic Properties of Materials by Time Domain Techniques," *IEEE Trans. Instrum. Meas.*, **IM-19**, 377–82 (1970).

[32] W. D. Kingery, H. K. Bowen, and D. R. Uhlman, *Introduction to Ceramics*, 2nd edition, Wiley, New York, 1976.

[33] J. A. Dean (ed.), *Lange's Handbook of Chemistry*, 12th edition, McGraw-Hill, New York, 1979.

[34] D. R. Lide (ed.), *CRC Hand Book of Chemistry and Physics*, 73rd edition, CRC Press, London, 1993.

[35] R. C. Buchanan, "Properties of Ceramic Insulators"; pp. 1–64 in *Ceramic Materials for Electronics, Processing, Properties and Applications, Chapter 1*, 2nd edition, Edited by R. C. Buchanan. Marcel Decker Inc., New York, 1991.

[36] V. Raghavan, "Dielectric Materials"; pp. 380–92 in *Materials Science and Engineering—A First Course, Chapter 17*, 4th edition, Prentice-Hall of India (P) Ltd., New Delhi, 1998.

[37] J. Mangels and B. Mikijelj, "Ceramic Radomes for Tactical Missile Systems Available at http://www.cera dyne.com/uploads/Radome%20White%20Paper %20PDF.pdf (accessed November 11, 2009) ☐